3ème Conférence Internationale sur les Sciences Appliquées et l'Innovation (CISAI-2025)
Proceedings Book Series –PBS- Vol 25, 318-325

Effect of Operating Conditions on Reverse Electrodialysis Performances

Sarra Jomaa [1], Sonia Besbes [2], Habib ben Aissia [3]

National Engineering School of Monastir, Laboratory of Metrology and Energy Systems, University of Monastir
BP 56 Avenue Taher Hadded, Monastir 5000, Tunisia

Email 2 - soniabesbes767@gmail.com

***Abstract*— The reverse electrodialysis (RED) process enables the direct production of electricity from a salinity gradient. Despite recent substantial advancements in research on RED technology, researchers still want to enhance its efficiency. In this study, a numerical model was developed using Aspen Custom Modeler software to carry out a parametric study on the RED process. Two feed solutions of brackish (0.02M)/sea water (0.5M) and brackish (0.1M)/brine (5M) were considered for the high and low concentration compartments, respectively. The influence of spacer thickness and Reynolds number on gross and net power densities was assessed for the Fumasep (FAD/FKD) membrane. The results showed that using a thicker spacer (270 µm) with a low Reynolds number of 3.4 in the high compartment and a thinner spacer (150 µm) with a high Reynolds number of 20 in the low compartment led to a higher net power density of 6.74 ($W.m_{cp}^{-2}$) for the brackish (0.1M)/brine (5M) feed solution.**

***Keywords*— Reverse electrodialysis, Reynolds number, Spacer thickness, salinity gradient, Net power density.**

I. INTRODUCTION

The world's growing population is driving up global energy demand, which is typically met by fossil fuels. The push to reduce reliance on these conventional sources has led to the development of clean, sustainable energy sources like Salt Gradient Power (SGP), which harnesses the difference in salt concentration between two streams [1]. Reverse electrodialysis (RED) is a key technology for harvesting SGP, using ion exchange membranes to draw electrical energy from the chemical potential difference between two solutions. In the RED stack, the concentrated and dilute solutions circulate alternately between the cation exchange membrane (CEM) and the anion exchange membrane (AEM) which are respectively permeable to cations and anions. The membranes are separated by spacers to maintain the inter-membrane distance and to minimize polarization phenomena. The ionic current is converted into electric current at the electrodes. This current can then be collected by an external load. Investigations focus on factors influencing the efficacy of the RED, like ion exchange membranes [2], [3], spacers [4]-[6], feed solution concentration [7], [8], flow rates [9], [10].

The aim of this paper is to show how the spacer, solution concentration and flow rate affect the net power density of the reverse electrodialysis process. The RED stack will be operated with two different spacer thicknesses (150 µm and 270 µm), two solution gradients and different Reynolds numbers. The RED process was modelled using Aspen Custom Modeler software and the results have been validated in our previous work [11] against experimental data from the literature.

II. MATHEMATICAL FORMULATION

This document is a template. An electronic copy can be downloaded from the conference website. For

In this work a detailed mathematical model using Aspen Custom Modeler software developed in our previous work [11] was used. We investigate most of the phenomena occurring within the RED stack with particular attention to the underlying transport phenomena, electrical characteristics, and performance indicators.

A. Electrical variables

The potential difference generated across each cell pair was evaluated from the Nernst equation:

$$E_{cell}^{RED}(x) = \alpha_{CEM}\frac{RT}{F}\left[\frac{1}{z^+}ln\left(\frac{\gamma_{HC}^{Na^+}C_{HC}^{Na^+}(x)}{\gamma_{LC}^{Na^+}C_{LC}^{Na^+}(x)}\right)\right] + \alpha_{AEM}\frac{RT}{F}\left[\frac{1}{z^-}ln\left(\frac{\gamma_{HC}^{Cl^-}C_{HC}^{Cl^-}(x)}{\gamma_{LC}^{Cl^-}C_{LC}^{Cl^-}(x)}\right)\right] \quad (1)$$

ISSN: 2961-6611

With α_{CEM} and α_{AEM} are the permselectivities of the cation and anion membranes, respectively, R is the universal gas constant (8.314 $J.mol^{-1}.k^{-1}$), T is the temperature (K), F is the Faraday's constant (96,485 $C{\cdot}mol^{-1}$) γ is the activity coefficient, C is ion concentration ($mol{\cdot}m^{-3}$), and HC and LC are the high and low concentration compartments, respectively.
The current density was determined through an equivalent circuit as follows:

$$j(x) = \frac{\sum E_{cell}^{RED}(x)}{N_{RED}\, R_{i,RED} + R_L} \tag{2}$$

Where $\sum E_{cell}^{RED}$ is the sum of all the cell pair voltages drop (V), R_L is the external load ($\Omega{\cdot}m^2$), N_{RED} is the number of cell pairs and $R_{i,RED}$ is the internal resistance of one cell pair ($\Omega{\cdot}m^2$), that can be expressed as follows [12]:

$$R_{i,RED}(x) = R_{ohmic,RED}(x) + R_{non-ohmic,RED}(x) \tag{3}$$

$$R_{ohmic,RED}(x) = R_{AEM} + R_{CEM} + R_{HC}(x) + R_{LC}(x) = R_{AEM} + R_{CEM} + \frac{\delta}{\varepsilon^2 \sigma_{HC}} + \frac{\delta}{\varepsilon^2 \sigma_{LC}} \tag{4}$$

Where R_{AEM} and R_{CEM} are the membrane resistances ($\Omega\,.m^2$), R_{HC} and R_{LC} are the High and low compartment resistances ($\Omega.m^2$), ε is the porosity of the spacer, δ is the intermembrane distance (spacer thickness) (m), and σ_{HC} and σ_{LC} are the conductivities in high and low concentration compartments, respectively ($S.m^{-1}$).
The non-ohmic resistance is composed of resistance due to the concentration change in the bulk solution along the compartments between the inlet and the outlet, $R_{\Delta C}$, and resistance due to the concentration polarization, R_{BL}[11] .
The gross power density of a cell pair P_G ($W.m_{cp}^{-2}$) was calculated as the product of the output voltage E (V) and the current, I (A), divided by the number of membrane pairs, N_{RED} , and the effective area per membrane, A (m^2), as follows:

$$P_G = \frac{EI}{N_{RED} A} \tag{5}$$

The output voltage E (V) is described as follows:

$$E = \sum E_{cell}^{RED} - jR_{Stack} \tag{6}$$

The net power density ($W.m_{cp}^{-2}$) calculated as the following expression:

$$P_{net} = P_G - \frac{P_{pump,RED}}{N_{RED} A} \tag{7}$$

$P_{pump,RED}$ is the pumping power (W) calculated according to the following equation:

$$P_{pump,RED} = \frac{\Delta P_{HC} Q_{HC} + \Delta P_{LC} Q_{LC}}{\eta} \tag{8}$$

ΔP_{HC} and ΔP_{LC} are pressure drops (Pa) between the inlets and the outlets of the low and high concentration compartments for a spacer filled system [9]. Q_{LC} and Q_{HC} are the average high and low flow rates ($m^3.s^{-1}$). η is the pump efficiency (75%).
The Reynolds number was calculated taking into account the porosity of the volume filled by the spacer [11].

$$Re = \frac{2Q\rho}{\varepsilon b \mu} \tag{9}$$

ρ is the density of the solutions ($kg.m^{-3}$), Q is the flow rate ($m^3.s^{-1}$) is the dynamic viscosity ($kg.m^{-1}.s^{-1}$), ε is the spacer porosity, and b is the channel width (m).

ISSN: 2961-6611

B. Transport phenomena

The flux generated by ions across IEM in RED, moves from concentrate to diluate solutions as below:

$$J_{Na^+}(x) = \frac{j(x)}{F} + \frac{D_{NaCl}}{\delta_{CEM}}(C_{HC}^{Na^+}(x) - C_{LC}^{Na^+}(x)) \quad (10)$$

$$J_{Cl^-}(x) = \frac{j(x)}{F} + \frac{D_{NaCl}}{\delta_{AEM}}(C_{HC}^{Cl^-}(x) - C_{LC}^{Cl^-}(x)) \quad (11)$$

Where D_{NaCl} is the salt diffusivity ($m^2 s^{-1}$) , δ_{AEM} , δ_{CEM} (m), are the anion and cation membranes thicknesses.

Another transport phenomenon takes place inside a cell pair which is transport due to osmotic and electro-osmotic flux. Osmotic flux is the movement of water molecules across the membrane, which reduces the efficiency of the system (loss of salinity gradient). In RED when ions (Na^+, Cl^-) migrate across membranes to balance charges, they take water molecules with them (due to their hydration layer), this is the electro-osmotic flux. The later flux moves from the diluate to concentrate compartments and is described by the following equations:

$$J'_{H_2O}(x) = J'_{osm}(x) + J'_{elos}(x) \quad (12)$$

Where the osmotic flux is estimated as bellow:

$$J'_{osm}(x) = L_P^{CEM}[\nu RT(\varphi_{HC}^{CEM} C_{HC}^{Na^+}(x) - \varphi_{LC}^{CEM} C_{LC}^{Na^+}(x))] + L_P^{AEM}[\nu RT(\varphi_{HC}^{AEM} C_{HC}^{Cl^-}(x) - \varphi_{LC}^{AEM} C_{LC}^{Cl^-}(x))] \quad (13)$$

And electro-osmotic flux as:

$$J'_{elos}(x) = \frac{w J_{tot}(x) M_w}{\rho_w} \quad (14)$$

L_P^{CEM} and L_P^{AEM} are the water permeability coefficients of the cation exchange membrane (CEM) and Anion exchange membrane (AEM) respectively, ν is the van't Hoff coefficient, and φ is the osmotic coefficient calculated according to Pitzer model [13].The ratio $\frac{M_w}{\rho_w}$ is the water molar volume ($m^3 . mol^{-1}$) and w is the hydration number, which can be assumed to be 7 for NaCl. J_{tot} is the overall salt flux estimated as follows:

$$J_{tot}(x) = \frac{j(x)}{F} - \frac{2D_{NaCl}}{\delta_{IEM}}[(C_{HC}^{Na^+}(x) + C_{HC}^{Cl^-}(x)) - (C_{LC}^{Na^+}(x) + C_{LC}^{Cl^-}(x))] \quad (15)$$

Where δ_{IEM} is the membrane thickness, $\delta_{IEM} = \delta_{AEM} = \delta_{CEM}$.

Mass balances of salt and water along the channels of a RED system are expressed according to the following equations:

$$\frac{dC_{HC}^{Na^+}(x)}{dx} = -\frac{b}{Q_{HC}(x)} J_{Na^+}(x) - C_{HC}^{Na^+}(x) \frac{b}{Q_{HC}(x)} J'_{H_2O}(x) \quad (16)$$

$$\frac{dC_{HC}^{Cl^-}(x)}{dx} = -\frac{b}{Q_{HC}(x)} J_{Cl^-}(x) - C_{HC}^{Cl^-}(x) \frac{b}{Q_{HC}(x)} J'_{H_2O}(x) \quad (17)$$

$$\frac{dC_{LC}^{Na^+}(x)}{dx} = \frac{b}{Q_{LC}(x)} J_{Na^+}(x) + C_{HC}^{Na^+}(x) \frac{b}{Q_{LC}(x)} J'_{H_2O}(x) \quad (18)$$

$$\frac{dC_{LC}^{Cl^-}(x)}{dx} = \frac{b}{Q_{LC}(x)} J_{Cl^-}(x) + C_{LC}^{Cl^-}(x) \frac{b}{Q_{LC}(x)} J'_{H_2O}(x) \quad (19)$$

III. NUMERICAL DETAILS

The numerical model developed under Aspen Custom Modeler analysed a RED stack of 20 cell pairs and an active surface area of 200 cm^2. The channel's geometric dimensions are 0.32 m in length and 0.063 m in

ISSN: 2961-6611

width. The investigation involved examining the Fumasep membrane and two spacers with thicknesses of 270 µm and 150 µm in HC and LC compartments, respectively. Table 1 provides the membranes properties used in this study. The following concentrations were considered for the two feed solutions: brackish/sea water (0.02M/0.55 M) and brackish/brine water (0.1M/5 M).

TABLE I
PROPERTIES OF ION EXCHANGE MEMBRANES [11]

Membrane type	**Permselectivity**	**Water permeability ($ml \cdot m^{-2} \cdot h^{-1} \cdot bar^{-1}$)**	**Salt diffusivity ($m^2 \cdot s^{-1}$)**	**Resistance ($\Omega \cdot cm^2$)**	**Thickness (µm)**
Fumasep AEM (FAD)	0.95	22	$1.3\,10^{-11}$	0.89	82
Fumasep CEM (FKD)	0.95	22	$1.3\,10^{-11}$	0.89	82

Partial differential equations are solved using approximations based on a first order backward finite difference method. A one-dimensional approach along the cell length with co-current flow distribution of pure NaCl solutions was considered with a step of 0.004 m. Electrode systems with opposite reactions and a recirculating electrode rinse are used. No net chemical reactions take place and the Nernst voltages cancel each other out. Fig. 1 shows a schematic description of the reverse electrodialysis (RED) stack.

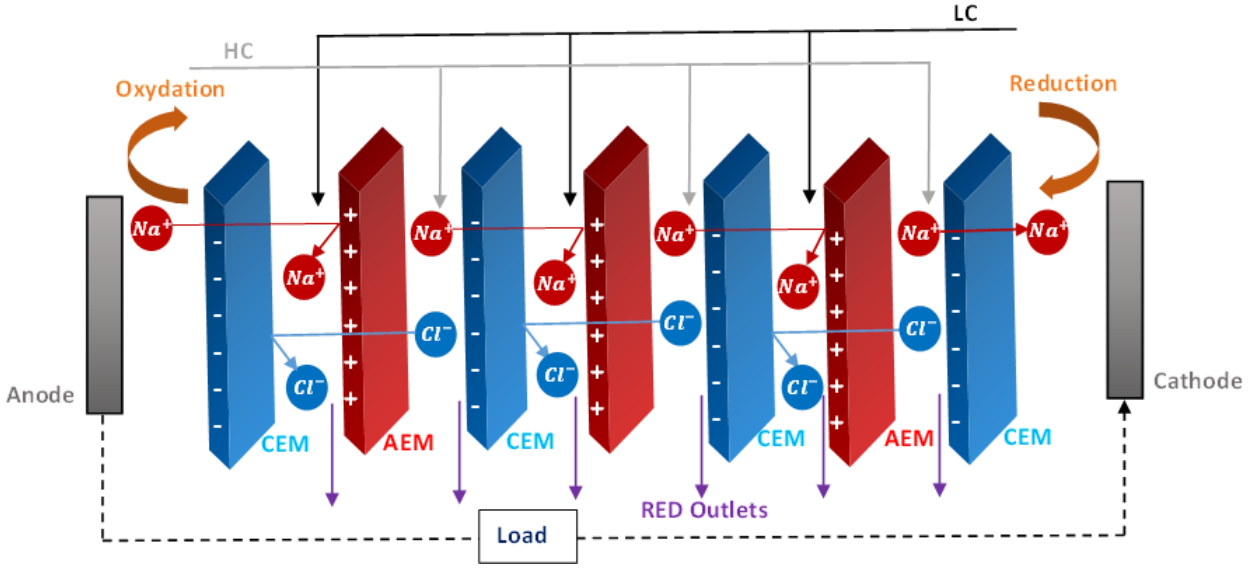

Fig.1 Schematic description of a RED stack. The HC and LC compartments are separated by alternated sequences of cation exchange membranes (CEMs) and anion exchange membranes (AEMs).

IV. RESULTS AND DISCUSSION

In the following section, we investigated the influence of flow rate (Reynolds number) on gross power density (GPD) and net power density (NPD). Initially, the Reynolds number was kept the same in both compartments. Then, we fixed the Reynolds number in the LC to a value of 7 and varied the Reynolds number in HC from 2.2 to 20. Finally, we fixed the Reynolds number in HC to a value of 3.4 and incremented the Reynolds number in LC up to 20. To further delve into the impact of spacers on the system's performance, we used different spacers' thicknesses in each channel while varying Reynolds number. As shown in Fig.2 (a), for brackish/sea water (0.02M/0.55 M), using a thicker spacer in HC and a thinner one in LC compartments led to low ohmic resistance. The high ohmic resistance obtained when δ_{sp_LC} = 270 µm is thus explained by the fact that the dilute compartment had a substantial impact on the internal resistance and that the smaller intermembrane distance reduced the dilute compartment's resistance. For $Re_{LC} = 7$ and $Re_{HC} = 3.4$, the dilute compartment's resistance constituted 40% of the total internal resistance when δ_{sp_HC} = 270 µm and δ_{sp_LC} = 150 µm while it was 51.66% when δ_{sp_HC} = 150 µm and δ_{sp_LC} = 270 µm. The effect of the

ISSN: 2961-6611

Reynolds number on the internal resistance shows that the higher Reynolds number in LC has a more pronounced impact on the internal resistance. Compared to seawater as a high-compartment solution (0.55M), the electrical resistance decreased by one order of magnitude with increasing salt concentration in the high compartment (5M) (Fig. 2(b)). The internal resistance of the Fumasep (FAD/FKD) membrane equals $5.35\,.10^{-4}$ ($\Omega \cdot m^2$) with (0.1M/5M) while it is $1.30\,.10^{-3}$ ($\Omega \cdot m^2$) with (0.02M/0.55M) when $Re_{LC} = Re_{HC} = 8.3$. The lowest ohmic resistance was obtained with low Reynolds numbers in the dilute compartment.

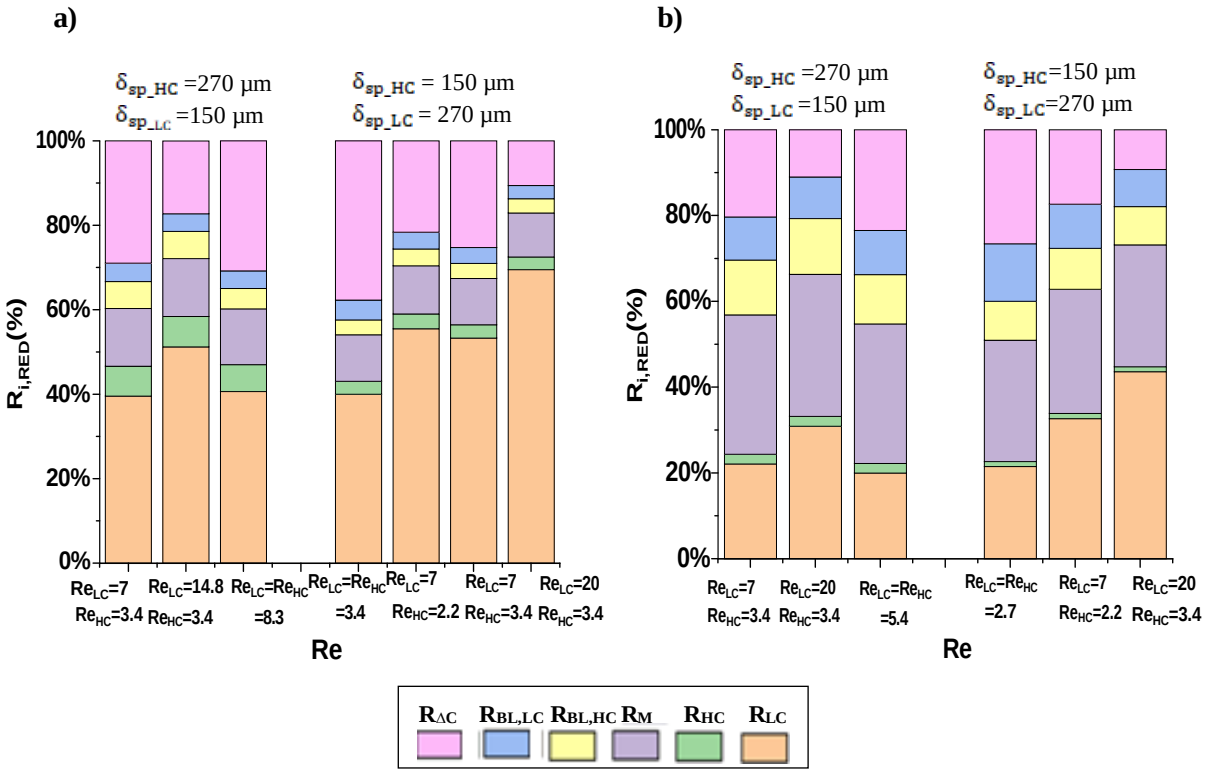

Fig.2. Internal resistance at maximum gross power when $Re_{LC} = or \neq Re_{HC}$, $\delta_{sp\ HC} \neq \delta_{sp\ LC}$, for Fumasep (FAD/FKD) membrane, (a) LC = 0.02M and HC = 0.55M; (b) LC = 0.1M and HC = 5M.

The gross power density (GPD), net power density (Net PD), and pump consumption are represented in Fig. 3(a-c) for the two feed solutions (brackish/sea water (0.02M/0.55 M) and brackish/brine (0.1M/5 M)), using a thicker spacer in HC (δ_{sp_HC} = 270 µm) and a thinner one in LC (δ_{sp_LC}=150 µm) compartments. This configuration of spacers led to low ohmic resistance, which is an important consideration in the field. As shown in Fig. 3(a), the GPD increases with increasing Reynolds number. In fact, at higher flow rates, the concentration change between HC and LC compartments decreases, resulting in a higher cell potential. Additionally, higher flow rates result in greater hydrodynamic losses due to pumping, which increases rapidly after a certain Reynolds number. Thus, the Net PD (which is the difference between the GPD and the power density due to pumping) increases until it reaches an optimal value and then decreases at a higher Reynolds number. When Re_{LC} was set to 7 and $Re_{HC}$was varied (Fig. 3(b)), the gross power density was less affected by the variation of the Reynolds number in the high compartment, and the highest net power density was obtained for low Reynolds numbers ($2.2 \leq Re_{HC} \leq 3.4$).

When $Re_{HC} = 3.4$ and $2.2 \leq Re_{LC} \leq 20$ (Fig.3(c)), the gross power density increased with the Reynolds number, while the increase in pumping power was less significant with a value that did not exceed 1($W \cdot m_{cp}^{-2}$), resulting in the highest net power density of 2.17 ($W \cdot m_{cp}^{-2}$), when mixing seawater with a salinity of 0.02 M and 6.74 ($W \cdot m_{cp}^{-2}$), for brine (HC = 5 M) and brackish water (LC = 0.1 M). In fact, the higher the salinity gradient, the higher the GPD and the Net PD, which is due to the decreased electrical resistance. These are the

ISSN: 2961-6611

highest values achieved and reported in the literature when mixing brine with brackish water (0.1 M/5 M) at T = 298 K.

a) $Re_{LC} = Re_{HC}$

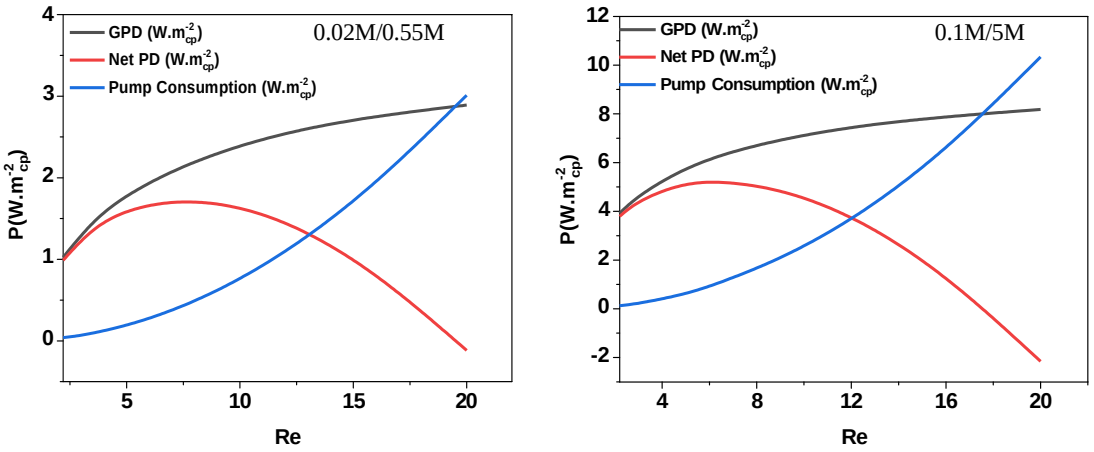

b) $Re_{LC} = 7$ and $2.2 \leq Re_{HC} \leq 20$

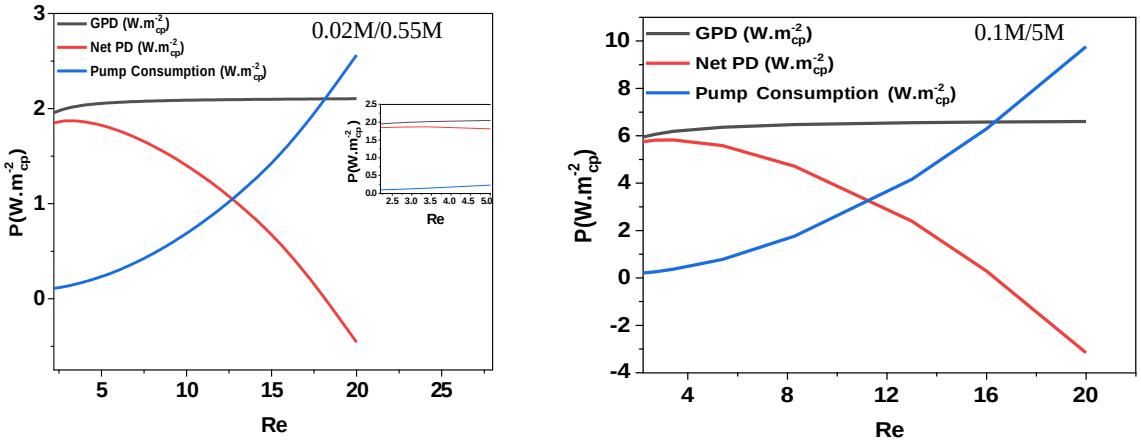

c) $Re_{HC} = 3.4$ and $2.2 \leq Re_{LC} \leq 20$

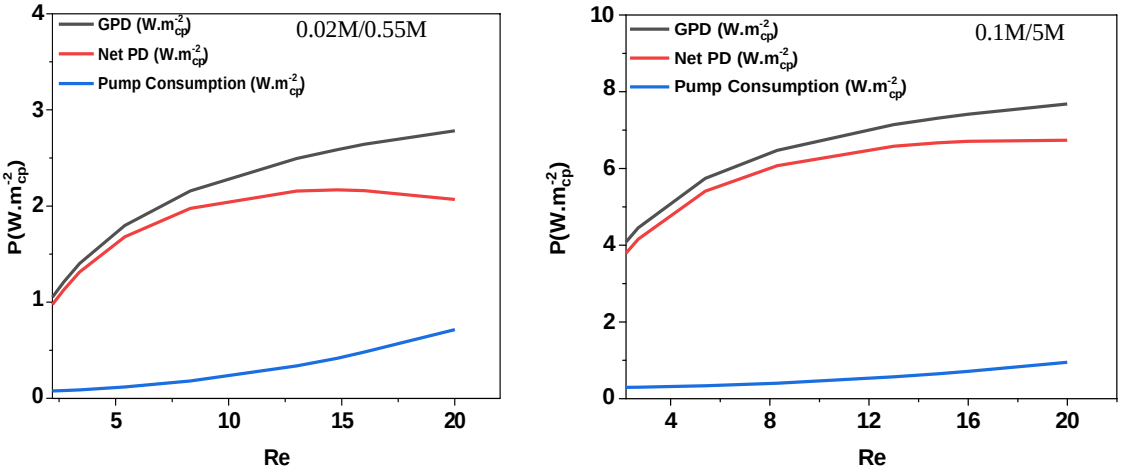

ISSN: 2961-6611

Fig.2. Gross power density (GPD), net power density (Net PD), and pump consumption, for the Fumasep (FAD/FKD) membrane, spacer thickness δ_{sp_HC} = 270 µm and δ_{sp_LC} = 150 µm, for brackish/sea water (0.02M/0.55M) and brackish/brine water (0.1M/5M).

IV. CONCLUSIONS

This paper investigated the effect of spacer thickness and Reynolds numbers on the gross and net power densities of the reverse electrodialysis (RED) process using a developed model with Aspen Custom Modeler software. Results showed that using a thinner spacer with high Reynolds numbers in the low compartment led to the highest net power density. The highest net power density achieved for the Fumasep membrane is 6.74 ($W \cdot m_{cp}^{-2}$) when using (0.1 M/5M) solutions, with Re_{HC}=3.4, Re_{LC}= 20, and δ_{sp_HC}=270 µm, δ_{sp_LC} =150 µm, at T=298K.

REFERENCES

[1] J. Veerman, M. Saakes, S. J. Metz, and G. J. Harmsen, "Reverse electrodialysis: Performance of a stack with 50 cells on the mixing of sea and river water," *J. Memb. Sci.*, vol. 327, no. 1–2, pp. 136–144, 2009, doi:10.1016/j.memsci.2008.11.015.

[2] M. Geise, M. A. Hickner, and B. E. Logan, "Ionic Resistance and Permselectivity Tradeoffs in Anion Exchange Membranes," 2013.

[3] E. Güler, R. Elizen, D. A. Vermaas, M. Saakes, and K. Nijmeijer, "Performance-determining membrane properties in reverse electrodialysis," *J. Memb. Sci.*, vol. 446, pp. 266–276, Nov. 2013, doi: 10.1016/J.MEMSCI.2013.06.045.

[4] J. W. Post, H. V. M. Hamelers, and C. J. N. Buisman, "Energy Recovery from Controlled Mixing Salt and Fresh Water with a Reverse Electrodialysis System," *Environ. Sci. Technol.*, vol. 42, no. 15, pp. 5785–5790, Aug. 2008, doi: 10.1021/ES8004317.

[5] J. Veerman, M. Saakes, S. J. Metz, and G. J. Harmsen, "Electrical Power from Sea and River Water by Reverse Electrodialysis: A First Step from the Laboratory to a Real Power Plant," *Environ. Sci. Technol.*, vol. 44, no. 23, pp. 9207–9212, Dec. 2010, doi: 10.1021/ES1009345.

[6] S. Mehdizadeh, M. Yasukawa, T. Abo, and Y. Kakihana, "E ff ect of spacer geometry on membrane and solution compartment resistances in reverse electrodialysis," *J. Memb. Sci.*, vol. 572, no. September 2018, pp. 271–280, 2019, doi: 10.1016/j.memsci.2018.09.051.

[7] R. Long, B. Li, Z. Liu, and W. Liu, "Performance analysis of reverse electrodialysis stacks : Channel geometry and fl ow rate optimization," *Energy*, vol. 158, pp. 427–436, 2018, doi: 10.1016/j.energy.2018.06.067.

[8] M. Micari *et al.*, "E ff ect of di ff erent aqueous solutions of pure salts and salt mixtures in reverse electrodialysis systems for closed-loop applications," *J. Memb. Sci.*, vol. 551, no. September 2017, pp. 315–325, 2018, doi: 10.1016/j.memsci.2018.01.036.

[9] J. Veerman, M. Saakes, S. J. Metz, and G. J. Harmsen, "Reverse electrodialysis: A validated process model for design and optimization," *Chem. Eng. J.*, vol. 166, no. 1, pp. 256–268, 2011, doi: 10.1016/j.cej.2010.10.071.

[10] M. Tedesco, H. V. M. Hamelers, and P. M. Biesheuvel, "Nernst-Planck transport theory for (reverse) electrodialysis: I. Effect of co-ion transport through the membranes," *J. Memb. Sci.*, 2016, doi: 10.1016/j.memsci.2016.03.012.

[11] S. Jomaa and S. Besbes, "Parametric analysis of reverse electrodialysis process for improved power generation: Influence of spacer thickness, feed solution flow rate, membrane, and concentration," *J. Water Process Eng.*, vol. 66, no. May, p. 106024, 2024, doi: 10.1016/j.jwpe.2024.106024.

[12] R. Ortiz-Imedio, L. Gomez-Coma, M. Fallanza, A. Ortiz, R. Ibañez, and I. Ortiz, "Comparative performance of Salinity Gradient Power-Reverse Electrodialysis under different operating conditions," *Desalination*, vol. 457, no. June 2018, pp. 8–21, 2019, doi: 10.1016/j.desal.2019.01.005.

[13] C. F. Weber, "Calculation of Pitzer parameters at high ionic strengths," *Ind. Eng. Chem. Res.*, vol. 39, no. 11, pp. 4422–4426, 2000, doi: 10.1021/ie000411o.1/ie000411o.

ISSN: 2961-6611